Title

Structural insights into the interaction of papain-like protease 2 from the alphacoronavirus porcine epidemic diarrhea virus and ubiquitin.

Journal

Acta Crystallographica Section D: Structural Biology, 77(Pt 7)

Authors

Durie, Ian

Dzimianski, John

Daczkowski, Courtney

et al.

Publication Date

2021-07-01

DOI

10.1107/S205979832100509X

Peer reviewed

STRUCTURAL BIOLOGY
ISSN 2059-7983

Structural insights into the interaction of papain-like protease 2 from the alphacoronavirus porcine epidemic diarrhea virus and ubiquitin

Ian A. Durie,[a] John V. Dzimianski,[a] Courtney M. Daczkowski,[a] Jack McGuire,[a] Kay Faaberg[b] and Scott D. Pegan[a]*

[a]Pharmaceutical and Biomedical Sciences, University of Georgia, 240 West Green Street, Athens, GA 30602, USA, and [b]Virus and Prion Research Unit, USDA–ARS–National Animal Disease Center, Ames, IA 50010, USA. *Correspondence e-mail: spegan@uga.edu

Received 2 April 2021
Accepted 13 May 2021

Edited by G. Cingolani, Thomas Jefferson University, USA

Keywords: PEDV; porcine epidemic diarrhea virus; ubiquitin; coronaviruses; deubiquitinases; papain-like protease 2.

PDB reference: PEDV papain-like protease 2 bound to ubiquitin, 7mc9

Supporting information: this article has supporting information at journals.iucr.org/d

Porcine epidemic diarrhea is a devastating porcine disease that is caused by the alphacoronavirus porcine epidemic diarrhea virus (PEDV). Like other members of the *Coronaviridae* family, PEDV encodes a multifunctional papain-like protease 2 (PLP2) that has the ability to process the coronavirus viral polyprotein to aid in RNA replication and antagonize the host innate immune response through cleavage of the regulatory proteins ubiquitin (Ub) and/or interferon-stimulated gene product 15 (ISG15) (deubiquitination and deISGylation, respectively). Because *Betacoronavirus* PLPs have been well characterized, it was sought to determine how PLP2 from the alphacoronavirus PEDV differentiates itself from its related counterparts. PEDV PLP2 was first biochemically characterized, and a 3.1 Å resolution crystal structure of PEDV PLP2 bound to Ub was then solved, providing insight into how *Alphacoronavirus* PLPs bind to their preferred substrate, Ub. It was found that PEDV PLP2 is a deubiquitinase and readily processes a variety of di-Ub linkages, in comparison with its *Betacoronavirus* counterparts, which have a narrower range of di-Ub activity but process both Ub and ISG15.

1. Introduction

Porcine epidemic diarrhea (PED) is a devastating porcine disease that causes severe gastroenteritis and is currently threatening the safety and economics of the United States pork industry. The causative agent of PED, porcine epidemic diarrhea virus (PEDV), is an enveloped, positive-sense single-stranded RNA (ssRNA) virus belonging to the *Alphacoronavirus* genus within the *Coronaviridae* family. PEDV was first observed in 1971 in the United Kingdom and continued to re-emerge through the years throughout Europe, causing mild outbreaks (Antas & Woźniakowski, 2019). It was not until 2010, when a new highly virulent strain of PEDV emerged in China, that cases began to be seen throughout the rest of the world. Cases of PEDV were first confirmed in North American swine in April 2013, and within just 14 months had spread to 30 different states, affecting almost 50% of swine herds and resulting in the loss of almost seven million pigs (Stevenson *et al.*, 2013; Goede *et al.*, 2015; Goede & Morrison, 2016). Compounding the devastation, PEDV has an astounding mortality rate of close to 100% in neonatal pigs (Stevenson *et al.*, 2013). Recently, it was estimated that the total economic impact in the US alone could range from an astonishing $900 million to $1.8 billion (Schulz & Tonsor, 2015; Paarlberg,

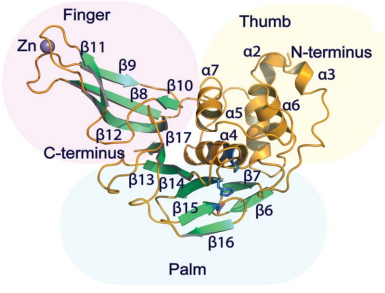

2014). Vaccines are currently available for PEDV; however, the efficacy and safety of these vaccines has recently been questioned (Song & Park, 2012; Song *et al.*, 2015; Subramaniam *et al.*, 2018). In addition, PEDV is often seen to co-infect with related coronaviruses that cause almost identical clinical symptoms, transmissible gastroenteritis virus (TGEV), porcine deltacoronavirus (PDCoV) and the newly emerged swine acute diarrhea syndrome coronavirus (SADS-CoV), which has caused complications in the diagnoses of these viruses (Zhang *et al.*, 2019). With continued outbreaks and re-emergence of PEDV and the emergence of new porcine coronaviruses, understanding how these viruses interact with their host will be key in the development of new therapeutics.

Coronaviruses (CoVs) are known to infect a wide variety of species, including mammals and birds, with viruses from the *Alphacoronavirus*, *Betacoronavirus* and *Deltacoronavirus* genera readily infecting pigs. The genome of PEDV is 28 kb in length and, like other positive single-stranded RNA viruses, encodes two cysteine proteases: the papain-like protease (PLP) and the 3C-like protease or main protease (3CLpro or M^{pro}). PEDV, as well as several other members of *Alphacoronavirus* and *Betacoronavirus*, encodes two copies of the PLP that are denoted PLP1 and PLP2; when a single PLP is encoded it is denoted PLpro (Woo *et al.*, 2012). Together, these proteases are responsible for the proteolytic processing of the long polyprotein into 16 different nonstructural proteins (nsps), which are essential for the formation of the membrane-bound replicase complex utilized during RNA replication (Thiel *et al.*, 2003; Barretto *et al.*, 2005; Ratia *et al.*, 2006; Mielech *et al.*, 2015; Harcourt *et al.*, 2004). The PLP is responsible for cleaving nsps 1–3, while the 3C-like protease cleaves nsps 4–16; however, the CoV PLP has been observed to play additional roles other than promoting viral replication (Barretto *et al.*, 2005; Ratia *et al.*, 2014).

Several CoV PLPs, such as the PLpros from severe acute respiratory syndrome coronavirus (SARS-CoV), severe acute respiratory syndrome coronavirus 2 (SARS-CoV-2), Middle East respiratory syndrome coronavirus (MERS-CoV) and avian infectious bronchitis virus (IBV) and the PLP2 from mouse hepatitis virus (MHV), have been suggested to downregulate the innate immune system by cleaving post-translational modifications of host proteins by ubiquitin (Ub) and Ub-like interferon-stimulated gene product 15 (ISG15) (Ratia *et al.*, 2006; Lindner *et al.*, 2007; Kong *et al.*, 2015; Freitas *et al.*, 2020). The processes of ubiquitination and ISGylation of viral and host proteins are essential for several pathways within the innate immune system, which is understood to be the first line of defense against viral infections (Davis & Gack, 2015; Sadler & Williams, 2008). As part of this defense, the induction of these pathways includes interferons (IFNs) within the type I interferon response (IFN-I), interferon-stimulated genes (ISGs) and cytokines as well as an inflammatory response through the NFκB pathway (Frieman *et al.*, 2009; Devaraj *et al.*, 2007). The combined activities of deubiquitination and deISGylation by PLP have been observed to antagonize the IFN-I response, suggesting that PLP is a virulence factor that can be manipulated for therapeutic purposes. This has been demonstrated through disruption of the deubiquitinating and deISGylating activities of MERS-CoV PLpro, which subsequently resulted in the partial suppression of Ub-dependent mitochondrial antiviral-signaling protein (MAVS)-mediated signaling, leading to the removal of the antagonized IFN-I response (Bailey-Elkin *et al.*, 2014). In addition, destabilizing mutations within MHV PLP2, which diminished both activities, resulted in a reversal of the antagonism of the IFN-I response (Mielech *et al.*, 2015). Taken together, these results demonstrate the need to further understand the PLPs from re-emerging CoVs, especially CoVs infecting swine such as PEDV, in order to better understand this key viral evasion mechanism and its associated pathogenicity.

The biochemically characterized CoV PLPs have been observed to possess varying degrees of deubiquitinase and deISGylase activities. Ubiquitination, and subsequent deubiquitinase activity, is not limited to a single mono-Ub event but includes polyubiquitination at one of the seven available lysine positions on Ub (positions 6, 11, 27, 29, 33, 48 and 63; Komander *et al.*, 2009; Kulathu & Komander, 2012). Both monoubiquitination and polyubiquitination of viral and host proteins are essential in several different signaling pathways. For example, Lys63-linked poly-Ub has been observed to be directly involved in the activation of retinoic acid-inducible gene I (RIG-I) and MAVS, which is a critical innate immune pathway in recognizing foreign single-stranded RNA (ssRNA; Faaberg *et al.*, 2006; Zeng *et al.*, 2010). Also, Lys48-linked poly-Ub has been observed to be involved in triggering the degradation of IκB in the NFκB pathway, and Lys11-linked poly-Ub has recently been implicated in TNF signaling (Alkalay *et al.*, 1995; Chen *et al.*, 1995; Castañeda *et al.*, 2013; Dynek *et al.*, 2010; Wang *et al.*, 2015). However, the exact role of deubiquitination activity in promoting CoV PLPs as antagonists of the IFN pathway is still unknown.

Work on PEDV PLP2 in cells has demonstrated that it is directly involved in the antagonism of the IFN response and can cleave poly-Ub chains from RIG-I and stimulator of interferon genes (STING); however, its exact catalytic activity and substrate preference have yet to be reported (Xing *et al.*, 2013). Here, the biochemical characterization of PLP2 from PEDV with regard to its deubiquitinating and deISGylating activities is described in detail. In addition, this study reveals the first structure of an *Alphacoronavirus* PLP2 bound to its preferred substrate, providing potential keys to understanding host–viral interactions.

2. Materials and methods

2.1. Expression and purification of the PLP2 domain of PEDV for biochemical characterization

The construct for the PLP2 domain originating from PEDV polyprotein 1a, consisting of residues 1616–1945 with an engineered 6×His tag, was cloned into the pET-15b expression vector (GenScript) and transformed into *Escherichia coli* BL21 (DE3) competent cells (New England Biolabs) via heat

shock. The cells were subsequently grown overnight in 250 ml LB broth supplemented with 100 µg ml^{-1} ampicillin at 37°C. 10 ml of the overnight culture was added to 1.5 l LB auto-induction medium (LB broth supplemented with β-lactose, glucose, glycerol, KH_2PO_4 and Na_2HPO_4, pH 8.0) and grown at 25°C for 24 h. The cells were collected via centrifugation at 10 000*g* for 15 min and stored at −80°C for purification. For purification, the cell pellets were resuspended in buffer *A* [5 *M* guanidine, 500 m*M* NaCl, 100 m*M* Tris pH 8.0, 10%(*v*/*v*) glycerol] supplemented with lysozyme. The cell suspension was then sonicated on ice at 80% power with a 50% duty cycle for a total of 8 min using a Fisher Scientific Series 150 cell disruptor. The cell lysate was centrifuged at 70 600*g* for 30 min at 4°C and the resulting supernatant was filtered using a 0.8 µm filter for further purification. The filtered supernatant was flowed over high-density nickel agarose beads (Gold Biotechnology) pre-equilibrated with cold buffer *A*, washed with 5 column volumes (CV) of buffer *A* supplemented with 30 m*M* imidazole and eluted with 5 CV buffer *A* supplemented with 300 m*M* imidazole. The eluted protein was dialyzed overnight in buffer *B* (1 *M* L-arginine, 100 m*M* NaCl, 100 m*M* Tris pH 8.0, 0.1 m*M* $ZnCl_2$) at 4°C and dialyzed a second time in buffer *C* [300 m*M* NaCl, 20 m*M* Tris pH 8.0, 0.1 m*M* $ZnCl_2$, 2 m*M* DTT, 5%(*v*/*v*) glycerol] for a minimum of 12 h to remove the L-arginine. The protein was further purified by size-exclusion chromatography using Superdex 200 resin (GE Healthcare) equilibrated with buffer *D* (150 m*M* NaCl, 10 m*M* HEPES pH 8.0, 0.1 m*M* $ZnCl_2$, 2 m*M* DTT). The fractions containing protein, as confirmed by SDS–PAGE, were pooled for biochemical assays.

2.2. Analysis of the enzymatic activity of PEDV PLP2 towards Ub and ISG15

To assess the steady-state kinetic parameters of PEDV PLP2, fluorescence assays were performed as described previously (Daczkowski *et al.*, 2017; Bester *et al.*, 2018; Deaton *et al.*, 2014). Briefly, purified PEDV PLP2 was tested against Ub, ISG15 and Z-RLRGG peptide conjugated to the fluorescent molecule 7-amino-4-methylcoumarin (AMC) and Lys11-, Lys48- and Lys63-linked di-Ub fluorescence resonance energy transfer (FRET) substrates (Boston Biochem). Assays were performed in duplicate in assay buffer [100 m*M* NaCl, 50 m*M* HEPES pH 7.5, 0.01 mg ml^{-1} bovine serum albumin (BSA), 5 m*M* DTT], with the change in relative fluorescence as a function of time (RFU min^{-1}) monitored within the steady-state region. For the di-Ub FRET assays, the turnover was determined by measuring the increase in fluorescence as a result of the separation of the FRET TAMRA–QXL pair, in which QXL acts as a quencher. Additional di-Ub FRET positions were tested that contained the fluorophore–quencher FRET pair in different positions to account for steric interference. The concentrations used in the assays were Ub-AMC and ISG15-AMC at 1 µ*M*, Z-RLRGG-AMC at 50 µ*M*, di-Ub FRET pairings at 1 µ*M* and PEDV PLP2 at 50 n*M*.

2.3. di-Ub cleavage assays

To perform the di-Ub cleavage assays, eight different di-Ub linkages, Lys6, Lys11, Lys27, Lys29, Lys33, Lys48, Lys63 and the N-terminal linear form, were purchased (Boston Biochem) to assess the ability of PEDV PLP2 to cleave the different di-Ub chains to mono-Ub. The assay was performed at 37°C in the above-mentioned assay buffer, minus BSA, with the substrates present at 10 µ*M* and PEDV PLP2 present at 100 n*M* in a total assay volume of 70 µl. The reactions were quenched with 9 µl 2× SDS–tricine sample buffer in a 1:1 ratio at seven different time points (0, 1, 2, 5, 10, 30 and 60 min) and were then boiled at 95°C for 5 min. Samples were analyzed by SDS–PAGE on a 10–20% Mini-Protean Tris–Tricine precast gel (Bio-Rad).

2.4. Expression and purification of the catalytic PLP2 domain of PEDV for complexation and crystallization

A shortened PLP2 domain (PEDV PLP2 short) without the ubiquitin-like domain (UBL; residues 1616–1690), consisting of residues 1691–1920 of the nsp3 from PEDV with an engineered 6×His tag, was cloned into the pET-15b expression vector (GenScript) and transformed into *E. coli* T7 Express competent cells (New England Biolabs) via heat shock. The cells were then grown overnight in 250 ml LB broth supplemented with 100 µg ml^{-1} ampicillin at 37°C. 10 ml of the overnight culture was added to 1.5 l LB broth and grown at 37°C until the OD of the culture reached 0.6. The culture was then induced with 0.5 m*M* isopropyl β-D-1-thiogalactopyranoside (IPTG) and incubated at 18°C overnight. The cells were collected by centrifugation at 5200*g* for 10 min and were stored at −80°C.

The cell pellet was resuspended in 125 ml lysis buffer (500 m*M* NaCl, 20 m*M* Tris pH 7.4, 10 m*M* β-mercaptoethanol) with lysozyme for 40 min. The cell suspension was then sonicated on ice at 50% power with a 50% duty cycle for a total of 6 min using a Fisher Scientific Series 150 cell disruptor. The lysate was then immediately centrifuged at 23 000 rev min^{-1} for 20 min. The supernatant was filtered using a 0.8 µm pore-size filter and the subsequent solution was poured over 2 ml high-density nickel agarose beads (Gold Biotechnology). The resin was subjected to 10 CV lysis buffer, 10 CV buffer supplemented with 10 m*M* imidazole and 10 CV buffer supplemented with 300 m*M* imidazole. The eluted protein was subsequently dialyzed in size-exclusion buffer (150 m*M* NaCl, 10 m*M* HEPES pH 7.4, 2 m*M* DTT, 0.1 m*M* $ZnCl_2$) overnight. The dialyzed protein was then injected onto a Superdex 75 size-exclusion column (GE Healthcare). The purity of the fractions was confirmed using gel electrophoresis.

2.5. Expression and purification of Ub for complexation

Ub (residues 1–75) in the vector pTYB2 was expressed, purified and derivatized with propargylamine to generate a suicide substrate (Ub-PA) as detailed previously (Deaton *et al.*, 2016). PEDV PLP2 short was saturated with Ub-PA and incubated at room temperature for 4 h. To remove excess Ub-PA, the complex was run over high-density nickel agarose

beads (Gold Biotechnology). The column was washed with 30 m*M* imidazole and was then eluted with 300 m*M* imidazole. Thrombin was added to the eluted fraction to remove the 6×His tag, and it was then dialyzed for 4 h in a buffer consisting of 150 m*M* NaCl, 25 m*M* HEPES pH 7.4, 2 m*M* DTT, 0.1 m*M* $ZnCl_2$. The protein complex was then concentrated to 6–7 ml and purified using a Superdex 200 size-exclusion column (GE Healthcare) in a running buffer consisting of 100 m*M* NaCl, 5 m*M* HEPES pH 7.4, 5 m*M* DTT, 0.1 m*M* $ZnCl_2$. The purity of the fractions was confirmed using gel electrophoresis.

2.6. Crystallization of PEDV PLP2 in complex with ubiquitin

The covalent PEDV PLP2 short–Ub complex was concentrated to 8.4 mg ml^{-1} and subsequently screened against 768 crystal conditions from a series of NeXtal suites using a Mosquito robot (TTP Labtech, Hertfordshire, UK). The screening used a 0.4 nl hanging drop comprised of a 1:1 ratio of protein solution and reservoir solution. Within 3–7 days, square plate crystals formed from a solution consisting of 0.2 *M* $MgCl_2$, 0.1 *M* Tris, 30% PEG 4K. The condition was further optimized by setting up trays with 500 µl well solution (0.30 *M* $MgCl_2$, 0.1 *M* Tris, 16% PEG 4K) and setting up a hanging drop that combined 2 µl well solution with 2 µl 9 mg ml^{-1} PEDV PLP2–Ub protein solution.

2.7. Data processing and structure solution

The crystals were flash-cooled in liquid nitrogen using 18% PEG 4K with 5% of a solution containing equal parts of ethylene glycol, DMSO and glycerol (EDG) as a cryoprotectant. Data were collected under a dry N_2 stream on the EIGER 16M detector at Brookhaven National Laboratory. The data set was indexed, integrated and scaled using *HKL*-2000 (Otwinowski & Minor, 1997). The structure was solved by molecular replacement with *Phaser* (McCoy *et al.*, 2007) using the solved apo structure of PEDV PLP2 (PDB entry 6noz; Center for Structural Genomics of Infectious Diseases, unpublished work). Successive rounds of manual model building and refinement were performed using *Coot* and *Phenix* (Emsley *et al.*, 2010; Liebschner *et al.*, 2019). Data-collection and refinement statistics are given in Table 1.

Table 1
Data-collection and refinement statistics.

Values in parentheses are for the highest resolution shell.

Wavelength (Å)	1.0
Resolution range (Å)	48.34–3.099 (3.210–3.099)
Space group	$P2_12_12_1$
a, *b*, *c* (Å)	98.138, 136.873, 193.348
α, β, γ (°)	90, 90, 90
Unique reflections	46738 (4185)
Multiplicity	6.1 (5.6)
Completeness (%)	97.21 (88.58)
Mean $I/\sigma(I)$	4.66 (1.0)
Overall *B* factor from Wilson plot	56.45
R_{merge}	0.231 (0.849)
R_{meas}	0.253 (0.936)
$R_{p.i.m.}$	0.102 (0.387)
$CC_{1/2}$	0.972 (0.614)
Reflections used in refinement	46723 (4182)
Reflections used for R_{free}	2349 (218)
Final R_{work}	0.2003 (0.2778)
Final R_{free}	0.2577 (0.3338)
No. of non-H atoms	
Total	19153
Macromolecules	19098
Ligands	46
Solvent	9
No. of protein residues	2465
R.m.s.d., bonds (Å)	0.007
R.m.s.d., angles (°)	0.40
Ramachandran favored (%)	97.11
Ramachandran allowed (%)	2.89
Ramachandran outliers (%)	0.00
Rotamer outliers (%)	0.05
Clashscore	4.79
Average *B* factor (Å^2)	
Overall	53.91
Macromolecules	53.89
Ligands	63.94
Solvent	34.19

3. Results and discussion

3.1. The deubiquitinating and deISGylating activity of PEDV PLP2

Previously, viral deubiquitinases (DUBs) and deISGylases have been shown to vary in their substrate specificity even between viral strains (Deaton *et al.*, 2014; Freitas *et al.*, 2020). To investigate the substrate preferences of PEDV PLP2, the full-length protease containing both the catalytic domain and the UBL was expressed and purified. Single-point kinetic parameters were assessed utilizing a 7-amino-4-methylcoumarin (AMC) fluorophore conjugated to the C-terminal end of Ub, human ISG15 and a short peptide sequence, RLRGG, which is the shared recognition sequence of the two prior substrates. The peptide is used as a control in order to examine the overall catalytic efficiency of the protease. The deubiquitinating and deISGylating substrate preferences were determined by monitoring the release of the AMC fluorophore over time. Curiously, PEDV PLP2 turns over Ub-AMC at 0.29 ± 0.0014 min^{-1}, which is three orders of magnitude above the rate of the deISGylase activity at (3.2 ± 0.039) × 10^{-4} min^{-1} (Figs. 1*a* and 1*b*). The overall peptide-AMC activity is similar to its deISGylase activity and was assessed as 1.0 × 10^{-2} min^{-1} (Fig. 1*c*). PEDV PLP2 appears to principally be a DUB, which intriguingly sets it apart from the PLpros from its *Betacoronavirus* counterparts SARS-CoV-2 and MERS-CoV. In comparison to other DUBs at the same substrate concentration, PEDV PLP2 has a similar DUB activity to SARS-CoV-2 PLpro, while its deISGylase function resembles that of the vOTU domain of porcine reproductive and respiratory syndrome virus modified live vaccine (PRRSV-MLV; Ingelvac PRRS MLV; Bester *et al.*, 2018).

3.2. Structure of PLP2 from the alphacoronavirus PEDV

With limited structural information available on PEDV PLP2 and how it engages with its preferred substrate, a structure of the protease complex was sought. Initial attempts to crystallize full-length PEDV PLP2 with or without Ub proved unsuccessful. However, screening just the catalytic

core (PEDV PLP2 short) with the Ub-PA substrate yielded a data set to 3.1 Å resolution. Using molecular replacement with a previously deposited unbound PEDV PLP2 short structure, a structural solution was found in space group $P2_12_12_1$. The asymmetric unit contained eight copies of the protease–Ub complex along with 14 zinc ions. A *DSSP* analysis of the catalytic core of PEDV PLP2 short reveals a mixture of seven α-helices, three 3_{10}-turns and 17 β-strands (Figs. 2 and 3*a*).

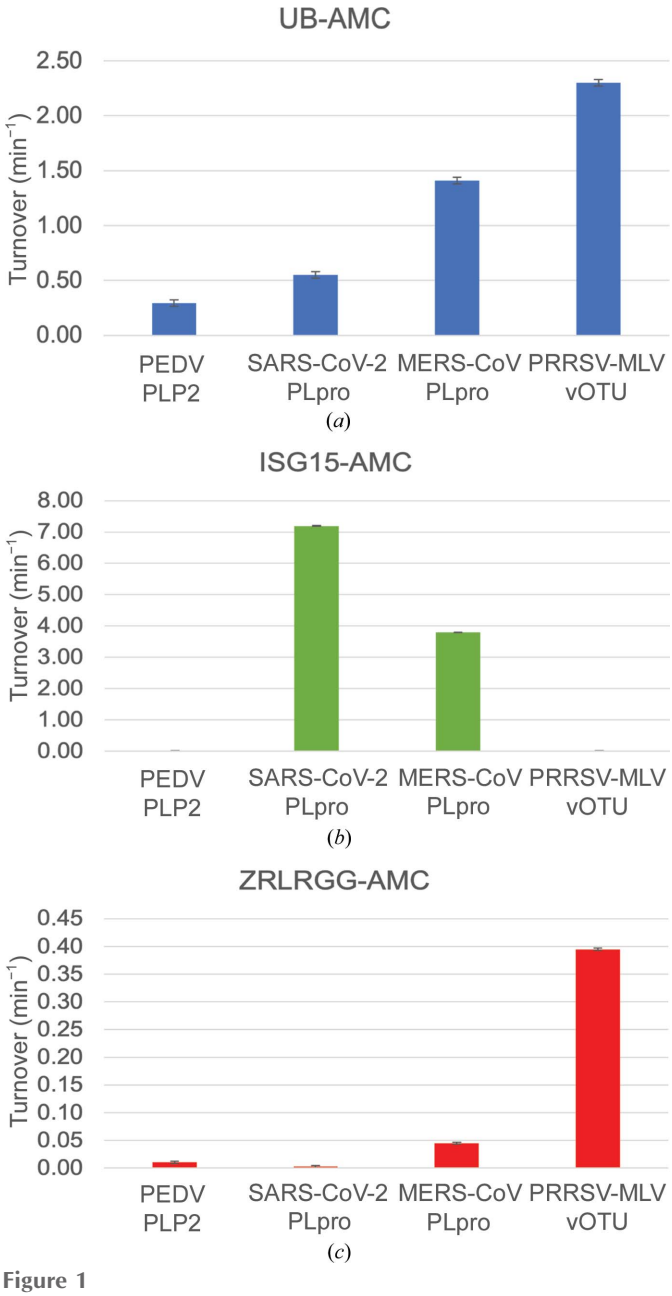

Figure 1
Comparison of the enzymatic activities of deubiquitinating enzymes. Protease activity of PEDV PLP2 in comparison to SARS-CoV-2 PLpro, MERS-CoV PLpro and PRRSV-MLV vOTU. All enzymes were assessed utilizing single concentrations of (*a*) 1 µ*M* Ub-AMC, (*b*) 1 µ*M* ISG15-AMC and (*c*) 50 µ*M* ZRLRGG-AMC. Readout is measured as the increase in fluorescence over time and is reported as turnover (molecules min^{-1}). Error is reported as the standard deviation. Specific activity data were taken from Freitas *et al.* (2020), Daczkowski *et al.* (2017) and Bester *et al.* (2018).

Eight of the zinc ions were associated with the finger domain of PEDV PLP2, whereas six zinc ions formed electrostatic bridges between the chains of PEDV PLP2. Four of the zinc ions formed bridges between the cloning remnant His-3 and His1692 of chains *A*, *C*, *G* and *E* and Cys1812 of chains *O*, *M*, *I* and *K* (Fig. 3*c*). The other two zinc ions formed bridges between Glu1803 and Cys1812 in chains *C* and *E* and Glu1803 and Cys1812 in chains *A* and *G* (Fig. 3*c*). An overlay comparison of the eight copies revealed very little global structural difference between the chains (Fig. 3*b*).

Overall, the secondary-structure elements of PEDV PLP2 give rise to the classic features of the catalytic domain of *Coronaviridae* PLPs (the finger domain, palm domain and thumb domain; Fig. 3*a*). As for other *Coronaviridae* PLPs, such as those from MERS-CoV and SARS-CoV, PEDV PLP2 can assume two states: an open state when unbound and a closed state when bound to substrate (such as Ub or ISG15; Bailey-Elkin *et al.*, 2014; Daczkowski *et al.*, 2017). To ascertain the common features and points of difference that can occur within *Alphacoronavirus* PLPs, our closed-conformation PEDV PLP2 structure and an open-conformation PEDV PLP2 structure (PDB entry 6noz) were overlaid with the recently solved structure of PLP2 from the alphacoronavirus swine acute diarrhea syndrome coronavirus (SADS-CoV; PDB entry 6l5t; Wang *et al.*, 2020) (Fig. 3*d*). Both *Alphacoronavirus* PLP2 structures were solved without their UBL domain, and the overlay shows that *Alphacoronavirus* PLP2s have similar secondary structures. SADS-CoV and PEDV PLP2 have 44% pairwise identity. Even though *Coronaviridae* PLPs have similar functions and folds, a difference in sequence identity can drastically change the binding affinity of a PLP for ISG15 and Ub. The finger and palm domains contain key regions that are responsible for the binding of Ub. The overlay of SADS-CoV and PEDV PLP2 shows some differences between the two structures, particularly in the finger domain.

SADS-CoV and PEDV PLP2 both contain six α-helices, while PEDV PLP2 has 12 β-strands in comparison to the 13 β-strands in SADS-CoV PLP2, which comprise the palm, finger and thumb domains. They both contain four β-strands that form the finger domain. In comparison with the proteases from betacoronaviruses and deltacoronaviruses, the finger domain does not appear to pack as tightly against the hydrophobic region in the palm domain (Daczkowski *et al.*, 2017). Within the finger domain, β-strands 11 and 12 contain a Cys1810–Cys1811–Cys1836–His1838 motif that binds to a Zn^{2+} ion. This is conserved among *Alphacoronavirus* proteases, in comparison to those from betacoronaviruses and deltacoronaviruses, which have a zinc-finger binding motif that is formed by four cysteine residues. The loop between β-strands 8 and 9 has some differences that affect the zinc-binding motif. Although they both contain a Cys–Cys–Cys–His motif that binds to a Zn^{2+} ion, SADS-CoV PLP2 has two additional amino acids, aspartic acid and arginine, that reside between Cys1810 and Cys1811 in PEDV PLP2 (Fig. 2). Both PLP2s have an aspartic acid residue in hydrogen-bonding proximity to Cys1811, which appears to stabilize the loop between β-strands 8 and 9 when bound to Zn^{2+}. When comparing the

open and closed conformations of PEDV PLP2, there is a 2.95 Å shift in the finger domain when moving from the unbound to the bound conformation.

Moving away from the finger to the palm domain, there are an additional four amino acids between β-strands 12 and 13 in PEDV PLP2. As part of the palm domain, three of these amino acids compose a 3_{10}-helix between β-strands 12 and 13. *Coronaviridae* PLPs have a highly conserved α-helix within the palm domain, denoted α-helix 4 in Fig. 2. This α-helix is in proximity to the catalytic triad denoted by Cys1729, His1888 and Asp1901, and contains Trp1730, which is conserved among PLPs from PEDV, SADS-CoV and human coronavirus (HCoV). In betacoronaviruses the tryptophan is replaced with a tyrosine, which can be exploited as an anchor for drug inhibition (Freitas *et al.*, 2020). With the subtle differences between SADS-CoV and PEDV PLP2, this replacement could result in a difference in affinity for Ub and ISG15.

3.3. Interaction of ubiquitin with PEDV PLP2

Previous work used the suicide substrate Ub-PA to covalently bind to PLPs and other deubiquitinases to aid in the study of their interactions with Ub (Capodagli *et al.*, 2013; Daczkowski *et al.*, 2017). Upon obtaining the first structure of an *Alphacoronavirus* PLP2 bound to the suicide substrate Ub-PA, we observed three main regions that confer important binding interactions: the finger domain, a hydrophobic region located in the palm domain, and the ubiquitin-binding site LRLRG, which is also located in the palm domain (Fig. 4).

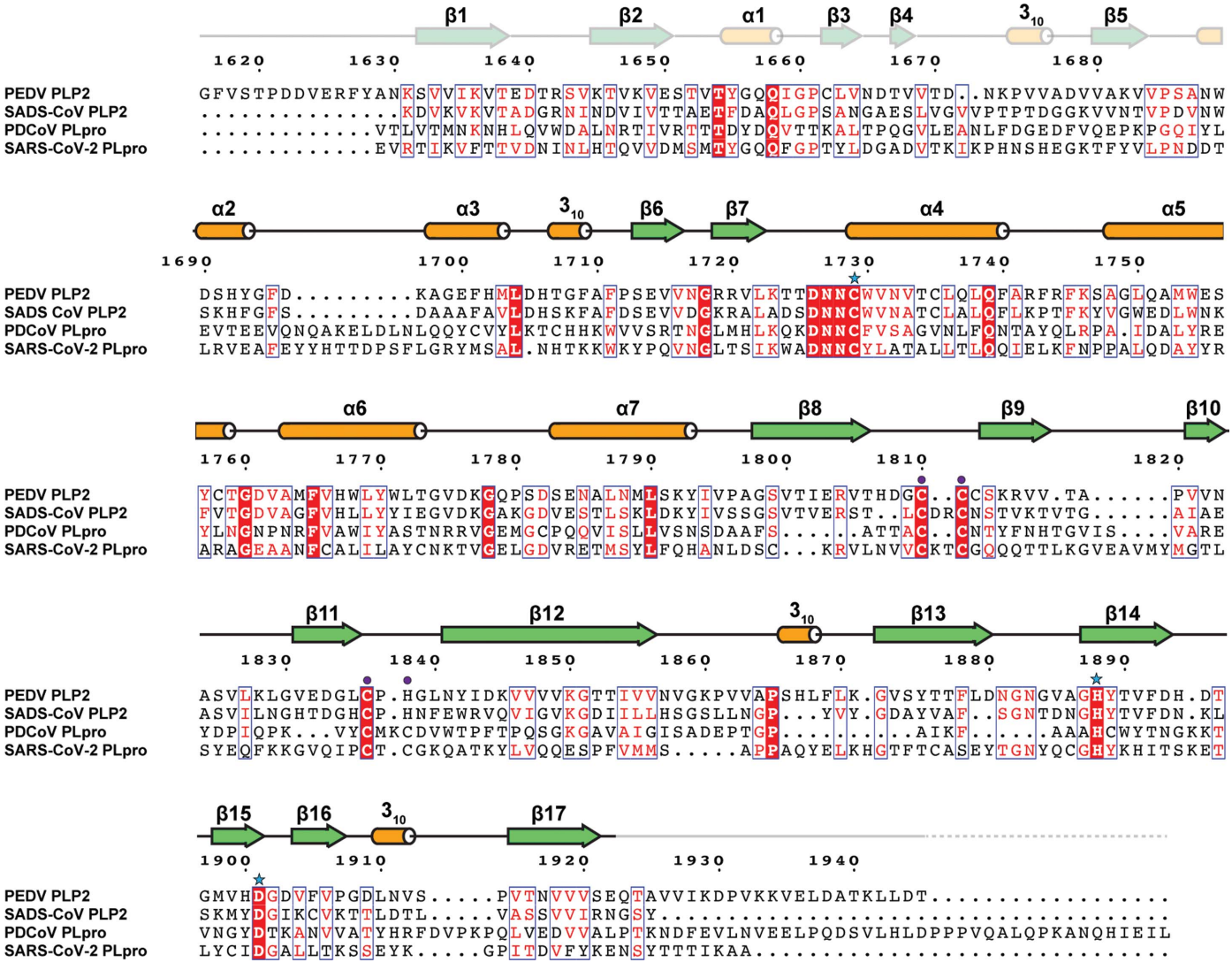

Figure 2
Sequence alignment of PLpros and PLP2s from coronaviruses: PEDV PLP2 (accession No. AHA38151.1), SADS-CoV PLP2 (accession No. ASK51716.1), PDCoV PLpro (accession No. AIP90485.1) and SARS-CoV-2 PLpro (accession No. QKG86869.1). The residue numbering is based on polyprotein 1a of PEDV. The faded secondary structure above the sequence alignment denotes the secondary structure of the UBL from SARS-CoV-2 PLpro (PDB entry 6w9c; Center for Structural Genomics of Infectious Diseases, unpublished work). The colored secondary structure was calculated by *DSSP* from experimental data and denotes the catalytic core that was used for crystallization. Residues that form the catalytic triad are denoted by sky blue stars, while the zinc-finger residues are marked by purple circles.

These three regions are also found in other PLPs and serve a similar function (Bailey-Elkin *et al.*, 2014; Békés *et al.*, 2016).

In the finger domain of PEDV PLP2, two interactions stand out in the interface with Ub. The first is the terminal N atom of Arg1815 of PEDV PLP2 located in β-strand 9, which interacts with Ala46 of Ub, and the second is an electrostatic interaction between Asp1833 of PEDV PLP2 in β-strand 11 and His68 of Ub-PA (Fig. 4*b*). Asp1833 is conserved among the PLP2s from the alphacoronaviruses SADS-CoV and PEDV. The electrostatic interaction between Asp1833 and His68 forces a conformational shift of β-strand 11 towards Ub-PA, which leads to an energetically favorable interaction between the hydrophobic region of Ub-PA and the hydrophobic region of PEDV PLP2 denoted by residues 1821–1824 and 1855–1858 (Fig. 4*c*). These observed interactions between PEDV PLP2 and Ub can also provide initial insight into the low deISGylase activity of PEDV PLP2. For instance, the counterparts in ISG15 of His68 in Ub tend to be large bulky or hydrophobic residues such as phenylalanine, tyrosine and isoleucine that would be incompatible with Asp1833 in PEDV PLP2. Additionally, Ile44 and Val70 of Ub, which are responsible for the hydrophobic interface with PEDV PLP2, tend to be hydrophilic residues in ISG15. Specifically, the counterpart in ISG15 of Ile44 in Ub is typically a serine or threonine, whereas the counterpart in ISG15 of Val70 in Ub is typically an asparagine or a histidine.

The LRLRG tail of Ub-PA rests in the active site of PLP2 between the finger and hydrophobic regions. To facilitate Ub processing, the PEDV PLP2 catalytic triad consisting of Cys1729, His1888 and Asp1901 is responsible for the enzymatic mechanism of DUB activity. In the case of our substrate Ub-PA, only Cys1729 from PEDV PLP2 forms a covalent interaction, while His1888 and Asp1901 make no discernible interactions with the Ub-PA tail. Otherwise, the Ub-PA main chain contains five main interactions. Ser1781 forms three hydrogen-bonding interactions with Arg72 and Gly75 in the backbone of the Ub tail. The other two interactions involve a hydrogen-bond interaction between Arg74 in Ub-PA and Asp1887 in PEDV PLP2 and interactions between Asp1782 and the main chain of the Ub-PA tail (Fig. 4*d*).

To characterize the bound (closed) conformation of PEDV PLP2, an overlay with the deposited unbound (open) conformation of PEDV PLP2 (PDB entry 6noz) was computationally performed to visualize the differences between the open and closed conformations. As with other PLPs, three main areas are observed that contort to account for a closed

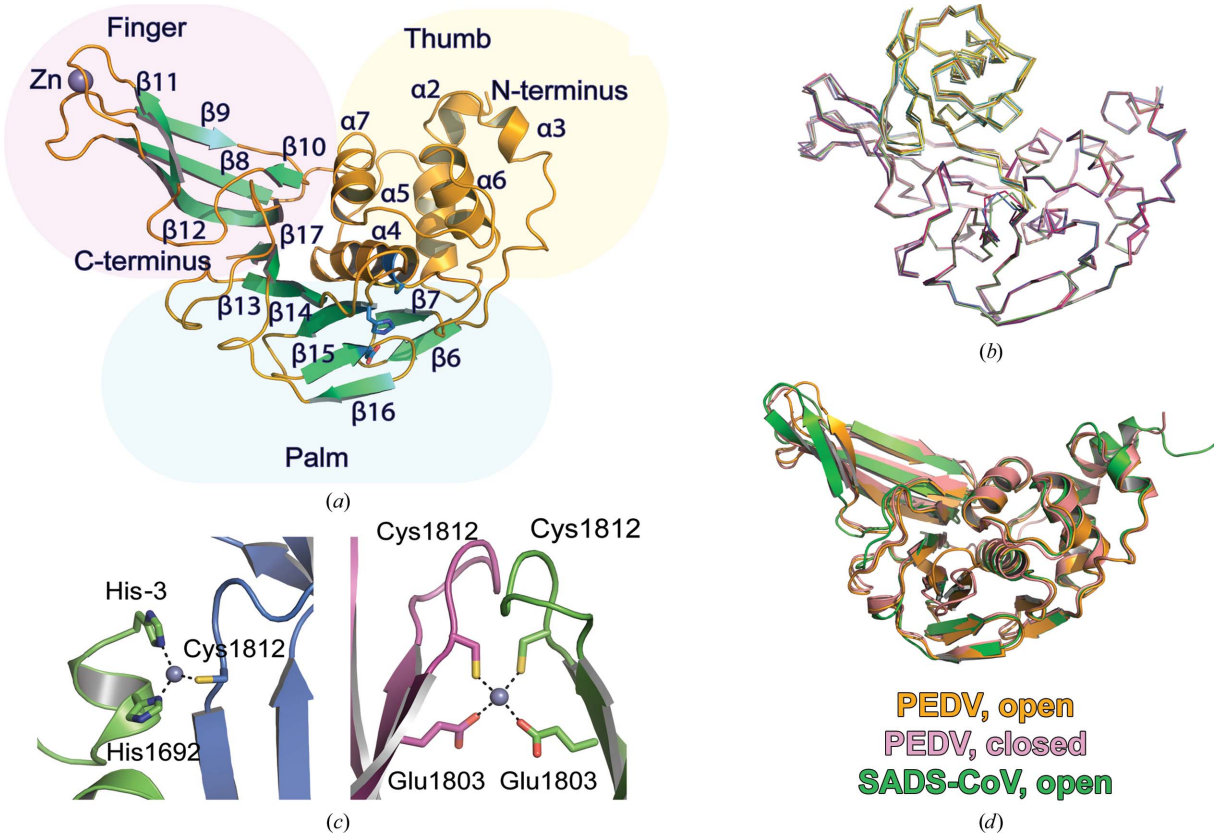

Figure 3
Structure of PEDV PLP2. (*a*) Cartoon rendering of PEDV PLP2 with α-helices in orange and β-strands in lime green; the catalytic triad is represented by sky blue sticks. The structural domains of PEDV PLP2 consist of the fingers (pale pink), palm (pale teal) and thumb (pale yellow) domains. (*b*) Ribbon overlay of the eight PEDV PLP2–Ub complex chains which make up the asymmetric unit. The r.m.s.d. of overlaid chains did not exceed 0.42 Å. (*c*) Zinc ion crystal contacts between chains in the asymmetric unit. (*d*) Overlay of open and closed PEDV PLP2 with SADS-CoV PLP2 (PDB entries 6noz and 6l5t). The r.m.s.d. of closed PEDV PLP2 to SADS-CoV PLP2 is 1.33 Å and that of closed PEDV PLP2 to open PEDV PLP2 is 0.9727 Å. Dashed lines represent hydrogen-bond distances of less than 3.5 Å.

conformation, as previously seen in bound PLPs (labeled I–III in Fig. 5; Daczkowski *et al.*, 2017). The finger binding domain moves towards the palm domain (I in Fig. 5). The shift of β-strands 11 and 12 towards the palm domain is facilitated by electrostatic interaction between Asp1833 of PEDV PLP2 and His6 of Ub. This movement forces a slight shift of β-strands 8 and 9 with the Zn^{2+} ion towards β-strands 11 and 12.

In the palm domain there are two main areas that constitute the closed conformation (II and III in Fig. 5): movement of the BL2 loop which occurs from binding of the Ub-PA tail to Cys1729 in the active site of PEDV PLP2. Some differences are usually found in the BL2 loop located between β-strands 14 and 15. The BL2 loop is usually observed to be highly flexible in many PLPs, and electron density does not usually appear unless it is influenced by the packing of the crystal lattice or the type of substrate bound. Surprisingly, the open conformation of PEDV yielded density to support how the BL2 loop moves (II in Fig. 5). When Ub-PA is locked into position, a similar conformation shift occurs as in the finger domain but with Arg74 of Ub and Asp1887 of PEDV PLP2. When moving from an open to closed conformation, Asn1883 moves 5.95 Å upwards towards the active site of PEDV PLP2 and the LRLRG tail of Ub.

These changes in conformation may help to account for the more stringent substrate specificity observed between the *Alphacoronavirus* and *Betacoronaviruses* PLPs. To obtain further insight into the closed conformation of bound PLPs, Ub-bound MERS-CoV PLpro, SARS-CoV-2 PLpro and our PEDV PLP2 structure were overlaid (Fig. 6). The overall folds of the three PLPs are nearly identical except for the finger domain. It appears that PEDV PLP2 is more rigid than its *Betacoronavirus* counterparts, including its finger domain and the BL2 loop. The finger domain of PEDV PLP2 does not move towards the palm domain nearly as much as those of SARS CoV-2 PLpro (PDB entry 6xaa; Klemm *et al.*, 2020) and MERS CoV PLpro (PDB entry 5v69; Zhang *et al.*, 2017). There is a dramatic shift of 16.45 Å from the closed PEDV PLP2 finger domain to the closed MERS CoV PLpro finger domain. This shift in the finger domain, alongside residue differences, could affect the substrate specificity for Ub and ISG15.

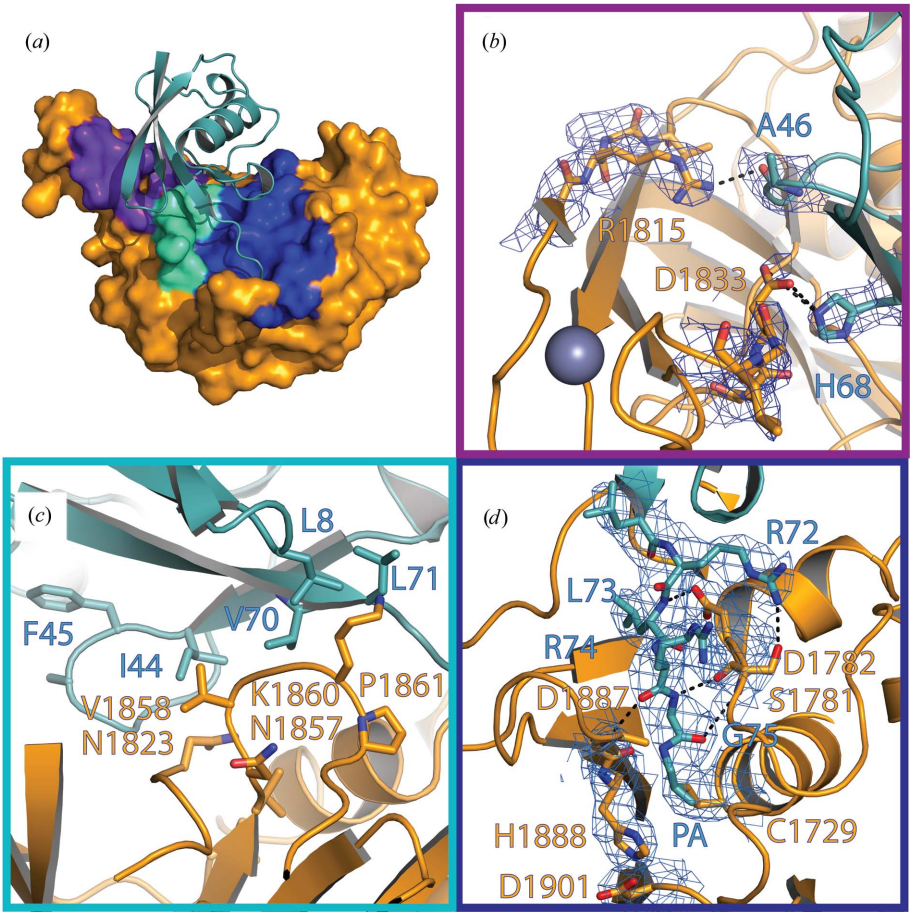

Figure 4
The PEDV PLP2 regions responsible for the binding of Ub. (*a*) Surface interactions of PEDV PLP2 with ribbon ubiquitin are shown in teal, with purple denoting the interaction of the finger domain with Ub, cyan denoting the interaction of the hydrophobic regions of PEDV PLP2 and Ub, and blue denoting the Ub tail binding site. (*b*) Hydrogen bonding between the finger domain and ubiquitin, with a $2F_o - F_c$ electron-density map overlaid over key residues. (*c*) Hydrophobic interactions between PEDV PLP2 and ubiquitin. (*d*) The partial ubiquitin recognition sequence LRLRG in the active site of PEDV PLP2 with a $2F_o - F_c$ electron-density map to show the key interactions in the active site. Dashed lines represent hydrogen-bond distances of less than 3.5 Å.

3.4. Polyubiquitin and PEDV PLP2

In some cases, DUBs can have higher turnover rates for poly-Ub linkages compared with mono-Ub, potentially due to an increase in favorable contacts with the larger Ub substrate (Capodagli *et al.*, 2013). To further investigate and characterize the DUB activity of PEDV PLP2, a panel of seven lysine-linked di-Ubs (at Lys6, Lys11, Lys27, Lys29, Lys33, Lys48 and Lys63) and linear di-Ub were tested by gel-shift assay (Fig. 7*a*). Over a span of 60 min, PEDV PLP2 was observed to have significant activity towards Lys63-, Lys48-, Lys11- and Lys63-linked di-Ub. In the past, PLPs have been observed to prefer Lys48-linked poly-Ub linkages (Freitas *et al.*, 2020; Ratia, 2008). Similarly, PEDV PLP2 was observed to have significant activity towards Lys48-linked di-Ub. Intriguingly, significant activity was also observed for Lys63-, Lys11- and Lys6-linked di-Ub, which shows similarity to the cleavage of Lys63- and Lys48-linked di-Ub by MERS-CoV PLpro and MHV PLP2 (Bailey-Elkin *et al.*, 2014).

After the initial di-Ub activity assays, Lys48- and Lys63-linked di-Ub fluorescence resonance energy transfer (FRET) substrates were used to quantify PEDV

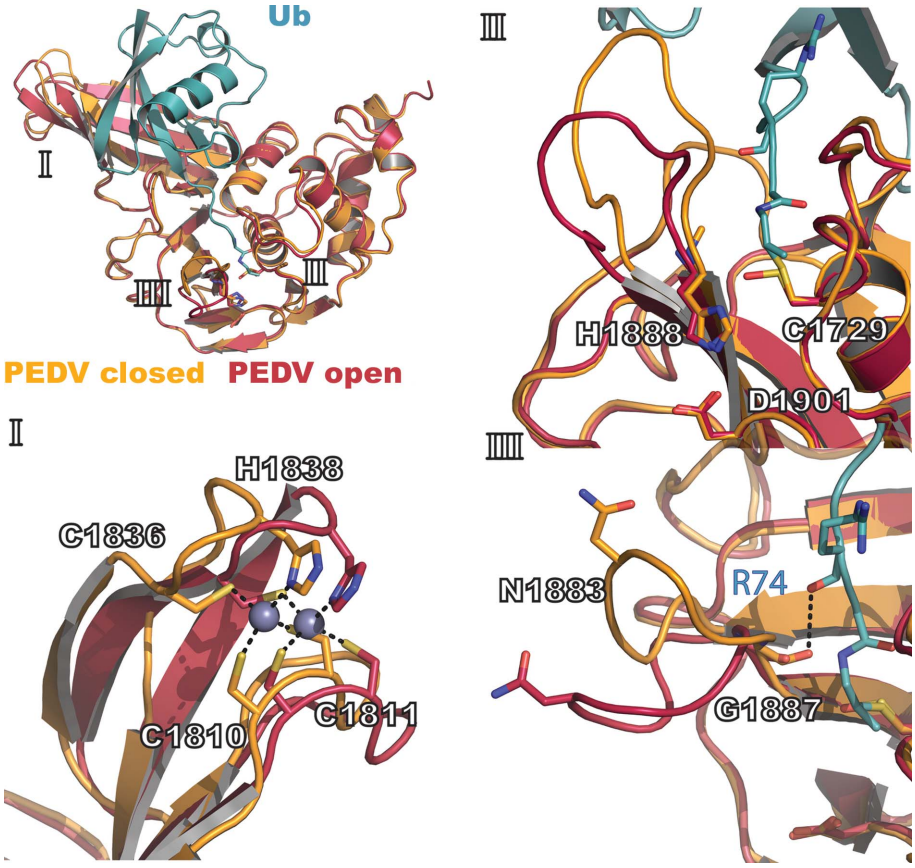

Figure 5
Closed versus open conformations of PEDV PLP2: comparison and overlay of closed and open PEDV PLP2 structures. I, zinc-finger movement. II, interactions of the PEDV PLP2 catalytic triad with RLRG of Ub. III, conformational changes of the BL2 loop with respect to the Ub RLRG tail. Dashed lines represent hydrogen-bond distances of less than 3.5 Å.

PLP2 activity. The activity towards each FRET substrate was monitored by an increase in fluorescence via the ability of the proteases to cleave the di-Ub molecule, which separates the FRET pairing. The overall di-Ub FRET activity of PEDV PLP2 was low for Lys48 and Lys63 linkages compared with that seen in cleavage assays using Ub-AMC and ISG15-AMC, likely suggesting that the FRET pair positioning interfered with the interaction of the protease with the substrates. Subsequent tests revealed that the positioning of the FRET pairing had a large impact on turnover, with preferences for position 4 for the Lys11 linkage, position 3 for the Lys48 linkage and position 3 for the Lys63 linkage (Fig. 7*b*).

Lys11-, Lys48- and Lys63-linked poly-Ubs have been strongly implicated as being involved in the antiviral innate immune response pathway, providing the potential link via which PLPs such as PEDV PLP2 can be involved in suppressing the innate immune response via deubiquitination. Specifically, Lys48-linked poly-Ub is responsible for activation of the inflammatory response through the NF-κB pathway via the proteasomal degradation of inhibitor of nuclear factor κB (IκB). Lys63-linked poly-Ub has been directly linked to antiviral signaling by RIG-I/MAVS, which induces type I IFNs (Daczkowski *et al.*, 2017; Deaton *et al.*, 2016; Zeng *et al.*, 2010). Finally, Lys11-linked poly-Ub has recently been shown to be involved in the ubiquitination of STING and TNF signaling, which induces pro-inflammatory cytokines in response to viral infection (Dynek *et al.*, 2010; Castañeda *et al.*, 2013).

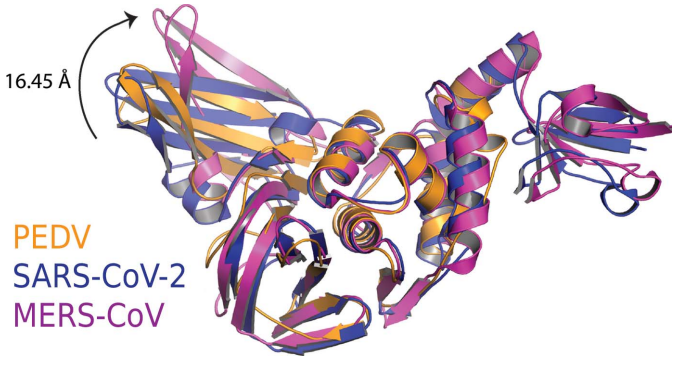

Figure 6
Closed conformations of PLPs. Comparison and overlay of bound (closed) PLPs. A mixture of *Alphacoronavirus* and *Betacoronavirus* PLPs bound to ubiquitin were overlaid on one another and the ubiquitin was removed to visualize the closed conformation of the PLPs. Our PEDV PLP2 structure was overlaid with those of PLpros from the betacoronaviruses SARS-CoV-2 (PDB entry 6xaa) in blue and MERS-CoV (PDB entry 5v69) in magenta. The r.m.s.d. of bound PEDV PLP2 to bound SARS-CoV-2 PLpro is 2.7 Å and that of bound PEDV PLP2 to bound MERS-CoV PLpro is 2.5 Å.

To obtain some insight in order to explain the substrate preferences of PEDV PLP2, we used our solved complex structure to overlay Lys48-linked di-Ub (PDB entry 5e6j; Békés *et al.*, 2016), Lys11-linked di-Ub (PDB entry 2mbq; Castañeda *et al.*, 2013) and Lys63-linked di-Ub (PDB entry 3h7p; Weeks *et al.*, 2009) (Fig. 7*c*). A previous study showed that Lys48-linked di-Ub makes a distinctive interaction with the UBL of SARS-CoV PLpro during crystal formation (Békés *et al.*, 2016). Although our construct did not express the PLP2 UBL, it appears that Lys48-linked di-Ub would play a role in forming interactions with the thumb domain. When Lys11-linked di-Ub was overlaid on our closed-conformation PEDV PLP2, significant interactions are seen with the distal Lys11-linked Ub, which interacts significantly with the finger and palm domains. The orientations of Lys63-, Lys48- and Lys11-linked di-Ubs do not sterically clash with our PEDV PLP2 structure. The ubiquitin binding is distinctive and different between coronaviruses, and the processing of Lys63-linked and Lys11-linked di-Ubs by PEDV PLP2 makes it

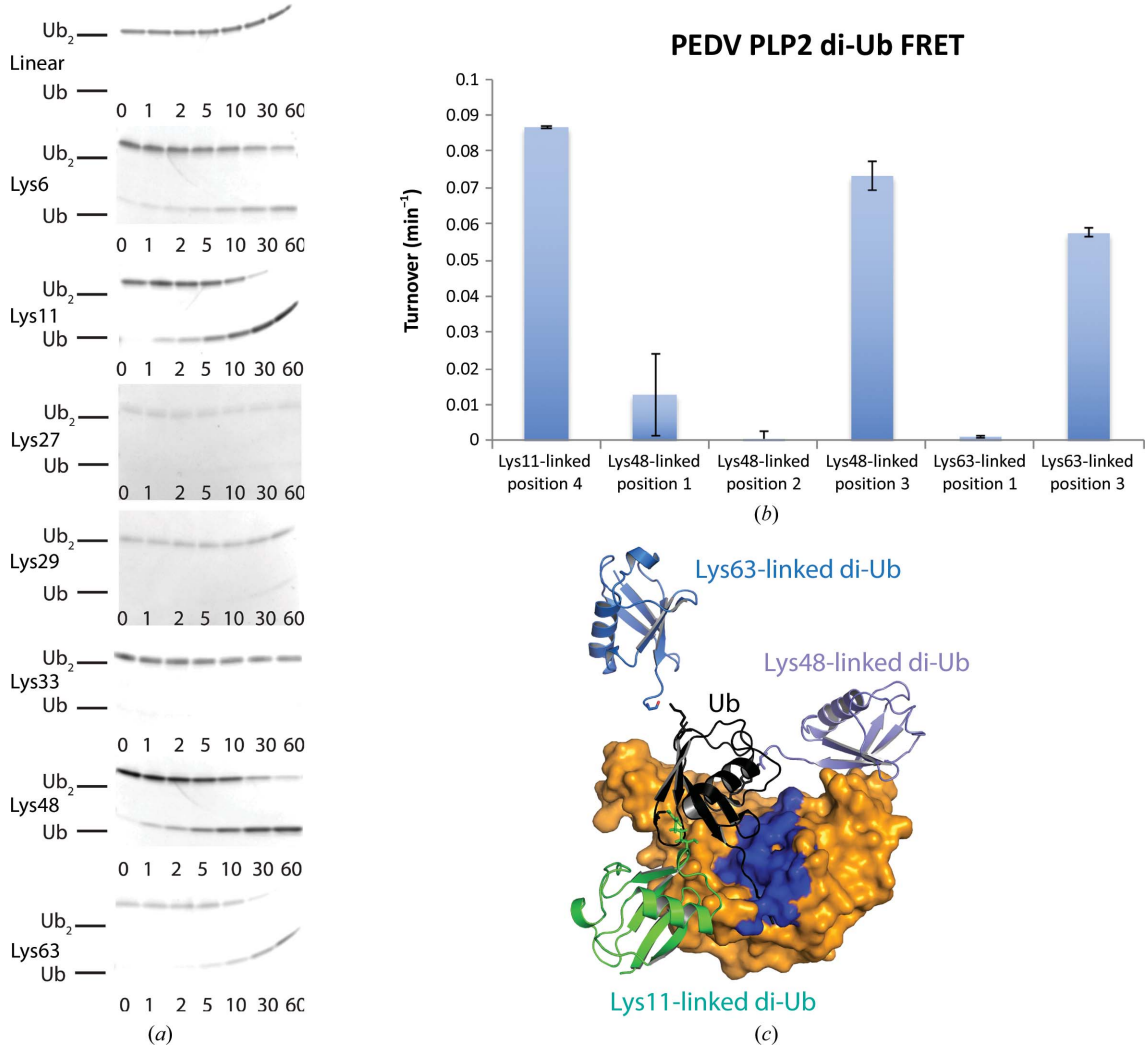

Figure 7
The ability of PEDV PLP2 to cleave di-Ub linkages. (*a*) Di-Ubs with various linkages (10 µ*M*) were incubated with PEDV PLP2 (200 n*M*) at 37°C for 60 min. Seven time points were taken and analyzed on a 10% Mini-Protean Tris–Tricine precast gel (Bio-Rad). (*b*) PEDV PLP2 was tested against di-Ub substrates. (*c*) Overlay of di-Ub substrates on bound PEDV PLP2. The blue region highlighted on the surface depicts the Ub binding site: Lys48-linked di-Ub from PDB entry 5e6j is in light purple, Lys11-linked di-Ub from PDB entry 2mbq is in light green and Lys63-linked di-Ub from PDB entry 3h7p is in light blue.

unique among coronaviruses. Taken together, the ability of PEDV PLP2 to process several different Ub linkages might suggest a link to the increased pathogenicity of PEDV.

4. Discussion and conclusion

Here, we report the first structure of an *Alphacoronavirus* PLP2 bound with the substrate Ub. As for other coronaviruses, we see a common theme among the PLPs, with Ub making significant interactions with the finger, palm and thumb domains. In comparison to *Betacoronavirus* PLPs, the finger domain of *Alphacoronavirus* PLPs has a less significant role in its interaction with Ub, which may explain its inability to process ISG15. The *Alphacoronavirus* PLP zinc-finger domain contorts itself away from Ub in comparison to structures such as those of MERS-CoV or SARS-CoV-2 PLpro bound to Ub or ISG15. This could explain its nonselectivity towards di-Ub linkages, with a preference for Lys63-, Lys11- and Lys6-linked molecules, while having an extremely low affinity for ISG15. The substrate specificity of Ub or ISG15 plays a major role in viral immune suppression, and the characterization of PEDV PLP2 may pave the way for further studies to fully understand its role in immune suppression.

Acknowledgements

This research used resources (beamline 17-ID-1) of the National Synchrotron Light Source II, a US Department of Energy (DOE) Office of Science User Facility operated for the DOE Office of Science by Brookhaven National Laboratory under Contract No. DE-SC0012704. The Center for Bio-Molecular Structure (CBMS) is primarily supported by the National Institutes of Health, National Institute of General Medical Sciences (NIGMS) through a Center Core P30 Grant (P30GM133893) and by the DOE Office of Biological and Environmental Research (KP1605010). X-ray data were

collected on the EIGER 16M detector at Brookhaven National Laboratory.

Funding information

The following funding is acknowledged: National Institute of Allergy and Infectious Diseases (grant No. R01AI151006 to Scott Pegan; award No. R01AI109008 to Scott Pegan); Agricultural Research Service (grant No. 58-5030-5034 to Scott Pegan, Kay Faaberg).

References

Alkalay, I., Yaron, A., Hatzubai, A., Orian, A., Ciechanover, A. & Ben-Neriah, Y. (1995). *Proc. Natl Acad. Sci. USA*, **92**, 10599–10603.

Antas, M. & Woźniakowski, G. (2019). *J. Vet. Res.* **63**, 465–470.

Bailey-Elkin, B. A., Knaap, R. C., Johnson, G. G., Dalebout, T. J., Ninaber, D. K., van Kasteren, P. B., Bredenbeek, P. J., Snijder, E. J., Kikkert, M. & Mark, B. L. (2014). *J. Biol. Chem.* **289**, 34667–34682.

Barretto, N., Jukneliene, D., Ratia, K., Chen, Z., Mesecar, A. D. & Baker, S. C. (2005). *J. Virol.* **79**, 15189–15198.

Békés, M., van der Heden van Noort, G. J., Ekkebus, R., Ovaa, H., Huang, T. T. & Lima, C. D. (2016). *Mol. Cell*, **62**, 572–585.

Bester, S. M., Daczkowski, C. M., Faaberg, K. S. & Pegan, S. D. (2018). *ACS Infect. Dis.* **4**, 1316–1326.

Capodagli, G. C., Deaton, M. K., Baker, E. A., Lumpkin, R. J. & Pegan, S. D. (2013). *J. Virol.* **87**, 3815–3827.

Castañeda, C. A., Kashyap, T. R., Nakasone, M. A., Krueger, S. & Fushman, D. (2013). *Structure*, **21**, 1168–1181.

Chen, Z., Hagler, J., Palombella, V. J., Melandri, F., Scherer, D., Ballard, D. & Maniatis, T. (1995). *Genes Dev.* **9**, 1586–1597.

Daczkowski, C. M., Goodwin, O. Y., Dzimianski, J. V., Farhat, J. J. & Pegan, S. D. (2017). *J. Virol.* **91**, e01067-17.

Davis, M. E. & Gack, M. U. (2015). *Virology*, **479–480**, 52–65.

Deaton, M. K., Dzimianski, J. V., Daczkowski, C. M., Whitney, G. K., Mank, N. J., Parham, M. M., Bergeron, E. & Pegan, S. D. (2016). *J. Virol.* **90**, 8314–8327.

Deaton, M. K., Spear, A., Faaberg, K. S. & Pegan, S. D. (2014). *Virology*, **454–455**, 247–253.

Devaraj, S. G., Wang, N., Chen, Z., Chen, Z., Tseng, M., Barretto, N., Lin, R., Peters, C. J., Tseng, C.-T. K., Baker, S. C. & Li, K. (2007). *J. Biol. Chem.* **282**, 32208–32221.

Dynek, J. N., Goncharov, T., Dueber, E. C., Fedorova, A. V., Izrael-Tomasevic, A., Phu, L., Helgason, E., Fairbrother, W. J., Deshayes, K., Kirkpatrick, D. S. & Vucic, D. (2010). *EMBO J.* **29**, 4198–4209.

Emsley, P., Lohkamp, B., Scott, W. G. & Cowtan, K. (2010). *Acta Cryst.* D**66**, 486–501.

Faaberg, K. S., Han, J. & Wang, Y. (2006). *Adv. Exp. Med. Biol.* **581**, 73–77.

Freitas, B. T., Durie, I. A., Murray, J., Longo, J. E., Miller, H. C., Crich, D., Hogan, R. J., Tripp, R. A. & Pegan, S. D. (2020). *ACS Infect. Dis.* **6**, 2099–2109.

Frieman, M., Ratia, K., Johnston, R. E., Mesecar, A. D. & Baric, R. S. (2009). *J. Virol.* **83**, 6689–6705.

Goede, D. & Morrison, R. B. (2016). *Prev. Vet. Med.* **123**, 202–207.

Goede, D., Murtaugh, M. P., Nerem, J., Yeske, P., Rossow, K. & Morrison, R. (2015). *Vet. Microbiol.* **176**, 161–164.

Harcourt, B. H., Jukneliene, D., Kanjanahaluethai, A., Bechill, J., Severson, K. M., Smith, C. M., Rota, P. A. & Baker, S. C. (2004). *J. Virol.* **78**, 13600–13612.

Klemm, T., Ebert, G., Calleja, D. J., Allison, C. C., Richardson, L. W., Bernardini, J. P., Lu, B. G., Kuchel, N. W., Grohmann, C., Shibata, Y., Gan, Z. Y., Cooney, J. P., Doerflinger, M., Au, A. E., Blackmore, T. R., van der Heden van Noort, G. J., Geurink, P. P., Ovaa, H., Newman, J., Riboldi-Tunnicliffe, A., Czabotar, P. E., Mitchell, J. P., Feltham, R., Lechtenberg, B. C., Lowes, K. N., Dewson, G., Pellegrini, M., Lessene, G. & Komander, D. (2020). *EMBO J.* **39**, e106275.

Komander, D., Clague, M. J. & Urbé, S. (2009). *Nat. Rev. Mol. Cell Biol.* **10**, 550–563.

Kong, L., Shaw, N., Yan, L., Lou, Z. & Rao, Z. (2015). *J. Biol. Chem.* **290**, 7160–7168.

Kulathu, Y. & Komander, D. (2012). *Nat. Rev. Mol. Cell Biol.* **13**, 508–523.

Liebschner, D., Afonine, P. V., Baker, M. L., Bunkóczi, G., Chen, V. B., Croll, T. I., Hintze, B., Hung, L.-W., Jain, S., McCoy, A. J., Moriarty, N. W., Oeffner, R. D., Poon, B. K., Prisant, M. G., Read, R. J., Richardson, J. S., Richardson, D. C., Sammito, M. D., Sobolev, O. V., Stockwell, D. H., Terwilliger, T. C., Urzhumtsev, A. G., Videau, L. L., Williams, C. J. & Adams, P. D. (2019). *Acta Cryst.* D**75**, 861–877.

Lindner, H. A., Lytvyn, V., Qi, H., Lachance, P., Ziomek, E. & Ménard, R. (2007). *Arch. Biochem. Biophys.* **466**, 8–14.

McCoy, A. J., Grosse-Kunstleve, R. W., Adams, P. D., Winn, M. D., Storoni, L. C. & Read, R. J. (2007). *J. Appl. Cryst.* **40**, 658–674.

Mielech, A. M., Deng, X., Chen, Y., Kindler, E., Wheeler, D. L., Mesecar, A. D., Thiel, V., Perlman, S. & Baker, S. C. (2015). *J. Virol.* **89**, 4907–4917.

Otwinowski, Z. & Minor, W. (1997). *Methods Enzymol.* **276**, 307–326.

Paarlberg, P. L. (2014). *Updated Estimated Economic Welfare Impacts Of Porcine Epidemic Diarrhea Virus (PEDV)*. Purdue University, USA.

Ratia, K. (2008). Thesis. University of Illinois at Chicago, USA.

Ratia, K., Kilianski, A., Baez-Santos, Y. M., Baker, S. C. & Mesecar, A. (2014). *PLoS Pathog.* **10**, e1004113.

Ratia, K., Saikatendu, K. S., Santarsiero, B. D., Barretto, N., Baker, S. C., Stevens, R. C. & Mesecar, A. D. (2006). *Proc. Natl Acad. Sci. USA*, **103**, 5717–5722.

Sadler, A. J. & Williams, B. R. (2008). *Nat. Rev. Immunol.* **8**, 559–568.

Schulz, L. L. & Tonsor, G. T. (2015). *J. Anim. Sci.* **93**, 5111–5118.

Song, D., Moon, H. & Kang, B. (2015). *Clin. Exp. Vaccine Res.* **4**, 166–176.

Song, D. & Park, B. (2012). *Virus Genes*, **44**, 167–175.

Stevenson, G. W., Hoang, H., Schwartz, K. J., Burrough, E. R., Sun, D., Madson, D., Cooper, V. L., Pillatzki, A., Gauger, P., Schmitt, B. J., Koster, L. G., Killian, M. L. & Yoon, K. J. (2013). *J. Vet Diagn. Invest.* **25**, 649–654.

Subramaniam, S., Yugo, D. M., Heffron, C. L., Rogers, A. J., Sooryanarain, H., LeRoith, T., Overend, C., Cao, D. & Meng, X.-J. (2018). *J. Gen. Virol.* **99**, 230–239.

Thiel, V., Ivanov, K. A., Putics, Á., Hertzig, T., Schelle, B., Bayer, S., Weissbrich, B., Snijder, E. J., Rabenau, H., Doerr, H. W., Gorbalenya, A. E. & Ziebuhr, J. (2003). *J. Gen. Virol.* **84**, 2305–2315.

Wang, D., Fan, J., Fang, L., Luo, R., Ouyang, H., Ouyang, C., Zhang, H., Chen, H., Li, K. & Xiao, S. (2015). *Mol. Immunol.* **68**, 357–366.

Wang, L., Hu, W. & Fan, C. (2020). *Protein Sci.* **29**, 1228–1241.

Weeks, S. D., Grasty, K. C., Hernandez-Cuebas, L. & Loll, P. J. (2009). *Proteins*, **77**, 753–759.

Woo, P. C. Y., Lau, S. K. P., Lam, C. S. F., Lau, C. C. Y., Tsang, A. K. L., Lau, J. H. N., Bai, R., Teng, J. L. L., Tsang, C. C. C., Wang, M., Zheng, B.-J., Chan, K.-H. & Yuen, K.-Y. (2012). *J. Virol.* **86**, 3995–4008.

Xing, Y., Chen, J., Tu, J., Zhang, B., Chen, X., Shi, H., Baker, S. C., Feng, L. & Chen, Z. (2013). *J. Gen. Virol.* **94**, 1554–1567.

Zeng, W., Sun, L., Jiang, X., Chen, X., Hou, F., Adhikari, A., Xu, M. & Chen, Z. J. (2010). *Cell*, **141**, 315–330.

Zhang, F., Luo, S., Gu, J., Li, Z., Li, K., Yuan, W., Ye, Y., Li, H., Ding, Z., Song, D. & Tang, Y. (2019). *BMC Vet. Res.* **15**, 470.

Zhang, W., Bailey-Elkin, B. A., Knaap, R. C. M., Khare, B., Dalebout, T. J., Johnson, G. G., van Kasteren, P. B., McLeish, N. J., Gu, J., He, W., Kikkert, M., Mark, B. L. & Sidhu, S. S. (2017). *PLoS Pathog.* **13**, e1006372.